Springer

KSME

Journal of Mechanical Science and Technology 31 (9) (2017) 4447~4458
www.springerlink.com/content/1738-494x(Print)/1976-3824(Online)
DOI 10.1007/s12206-017-0845-2

Multi-objective parameter space approach based controller and add-on disturbance observer design †

Mümin Tolga Emirler[1,*] and Bilin Aksun Güvenç[2,3]

[1]*Department of Mechanical Engineering, İstanbul Okan University, İstanbul, 34959, Turkey*
[2]*Automated Driving Lab in the Center of Automotive Research, The Ohio State University, Columbus, OH 43210, U.S.A.*
[3]*Department of Mechanical and Aerospace Engineering, The Ohio State University, Columbus, OH 43210, U.S.A.*

(Manuscript Received June 8, 2016; Revised January 11, 2017; Accepted May 23, 2017)

Abstract

The parameter space approach based robust PI control design methodology for DC motor speed control is proposed in this paper. The multi-objective design requirements like D-stability, phase margin and mixed sensitivity (frequency domain) bounds are mapped into the controller parameter space to determine PI controller coefficients which satisfies the desired user-defined specifications. Besides robust PI controller, an add-on disturbance observer is utilized to enhance the tracking performance and disturbance rejection of the control system. The proposed control scheme is validated by simulations and experiments. The results prove that the effectiveness of the proposed control system against uncertainties in the modeling and disturbances on the system response.

Keywords: DC motor speed control; Disturbance observer; Mixed sensitivity requirements; Parameter space approach; Robust control

1. Introduction

Direct current (DC) motors are essential parts of mechatronic and control systems. The use of DC motors in scientific research and industrial applications is very prevalent for their accurate and simple control characteristics. DC motors have been widely used in robotic applications, positioning systems, electric vehicles, flatbed scanners [1-5] and all sorts of rotational actuation processes.

One of the main challenges in DC motor speed control is to achieve stability and precise speed regulation even under uncertainties in the modeling and external disturbances [6, 7]. Generally, nominal model used in the design stage of the speed controller does not include high frequency dynamics (unmodeled dynamics) and also it suffers from the parametric variations due to the change of physical parameters in time. Another problem is the external disturbance (load torque) that affects the system response of DC motor. If the parametric variation, unmodeled dynamics and external disturbance do not take into consideration in the controller design stage, they may cause performance degradation and instability as a worst case [8].

There have been many contributions in the literature for DC motor control ranging from conventional PID control to advanced control methodologies such as sliding mode control, robust H_∞ control, LMI based robust control, adaptive control, intelligent control such as fuzzy logic, neural network and fractional order controllers.

In Ref. [8], sliding mode controller, integral sliding mode controller and dynamic sliding mode controller designs are represented for the DC motor speed control and the controllers are compared each other using simulation results with respect to their robustness against matched uncertainties and chattering reduction. Chattering is reduced with integral and especially dynamic sliding mode techniques. In Ref. [6], sliding mode control approach is applied to separately excited DC motor and the results are compared with the conventional PI controller using simulations. In Ref. [9], a sliding mode controller requiring only output feedback is proposed and verification with three different experiments on a DC motor speed control system is performed. A pre- and post-filtering approach to output feedback variable structure speed control of a permanent magnet DC motor is proposed and tested by simulations and experiments in Ref. [10]. In Ref. [11], a DC motor speed controller is proposed gathering the features of sliding mode control, fuzzy inference system, neural network and genetic algorithms in order to avoid the chattering disadvantage of sliding mode control. The designed controllers are implemented on a FPGA. The fluctuations in the conventional sliding mode controller results are reduced with sliding mode controller with adaptive neural fuzzy interference system and

*Corresponding author. Tel.: +90 212 677 2466, Fax.: +90 212 6771647
E-mail address: tolgaemirler@yahoo.com
† Recommended by Associate Editor Yang Shi

after the optimizing the fuzzy inference system with genetic algorithms the best final results are obtained.

A robust H_∞ optimal speed control scheme for a DC motor with parameter variations using a linear matrix inequality approach is introduced and tested by simulations in Ref. [12]. In Ref. [7], a mixed H_2/H_∞ robust controller design for DC motor speed control is presented and tested by simulations. Improved particle swarm optimization is used to solve the optimization problem of H_2/H_∞ controller and find the optimal parameters of the controller.

A robust adaptive discrete variable structure control scheme for DC motor speed control is described and successfully implemented in Ref. [13]. A self-tuning minimum variance adaptive control method is developed and successfully implemented for speed and position tracking of a DC motor in Ref. [14]. In Ref. [15], an online self-tuning artificial neural network based speed control scheme is proposed and experimentally implemented for a DC motor. The proposed scheme is compared with PI controller based system. The results show that the performance of artificial neural network based system is superior. An adaptive control algorithm using bacterial foraging algorithm for DC motor speed control is represented in Ref. [16]. In this research, bacterial foraging algorithm is used for identification and control of DC motor. A comparison of bacterial foraging algorithm based control and genetic algorithm based control is carried out. An adaptive PID-type neural network control method is applied for the speed control of a DC motor system dead-zone characteristics in Ref. [17]. A fractional order PI controller for controlling the speed of a DC motor was designed and implemented on a FPGA target in Ref. [18].

Disturbances exist in the DC motor systems inherently and externally originating from different sources such as load torque, friction, low-frequency vibration in the supporting structure, etc. [19]. They may occur as step disturbance or high-order disturbances such as ramp or parabola disturbances. Among high-order disturbances, ramp disturbances are especially important. The viscous friction which increases with the increase velocity under uniform accelerated motion is an example of ramp disturbance in the DC motor systems [20].

There are numerous papers in the literature to deal with the disturbance in the DC motor systems [6, 8, 13, 15, 19-24]. They use different approaches such as sliding mode control, artificial neural network based control, disturbance observer based control, sliding mode observer based model reference adaptive control, model reference fuzzy adaptive control.

In this paper, parameter space approach based robust PI controller design was carried out to control of DC motor speed considering multi-objective design requirements such as D-stability, phase margin bounds and mixed sensitivity (robust performance) requirements. The parameter space approach can be used to determine a set of coefficients for a given controller structure which simultaneously stabilize a finite number of plants. The set of parameters for which the characteristic polynomial is Hurwitz-stable is determined. Along with Hurwitz stability, the method has been extended to D-regions for treating relative stability and bandwidth constraints. The parameter space approach cannot handle only parametric (structured) uncertainties. By mapping frequency domain specifications into parameter space, the parameter space method provides the using of experience in the field of frequency domain robust control methods which generally tackle unstructured uncertainties such as H_∞ robust control. The further information about parameter space approach can be found at Refs. [25, 26]. The mapping of design requirements into the parameter space to find the robust fixed disturbance observer parameters was applied to vehicle yaw stability control successfully in earlier works [27-30]. In this paper, parameter space approach based design methodology used for designing robust PI controller. Also, an add-on disturbance observer employed to improve the tracking and disturbance rejection properties of the robust PI based control system. Robust PI and add-on disturbance designs were tested by simulations and experiments.

Some major robust control methods have already been applied to DC motor speed control. These methods can be categorized as linear and nonlinear control techniques. One of the most important nonlinear control technique applied DC motor speed control is sliding mode and related control methods [6, 8, 11]. Using sliding mode control, the bounded uncertainties and the external disturbance can be compensated. However, the main drawback of the sliding mode control is chattering resulting from nonlinear controllers. Chattering reduction can be achieved by improvements on the sliding mode control method [8], but this effect is not removed entirely. The main advantage of the proposed control system in this paper is that there is no chattering effect in this method.

Linear robust control techniques such as robust H_∞ optimal control method have also been applied to the DC motor speed control [7, 12]. A comparison of the parameter space approach and frequency domain approaches like robust H_∞ control optimal control can be done briefly as follows [26, 31]. The advantages of parameter space approach in comparison with $H\infty$ methods are: (i) The ease of visualization due to the graphical representation of the solution in parameter space, (ii) the determination of a solution region rather than one specific solution, (iii) obtaining fixed structure low order controller filters that are easily implementable. There are also some shortcomings of the parameter space approach in comparison to H_∞ methods such as: (i) The method can simultaneously accommodate the design of only two to three controller parameters due to its graphical display of the solution region, (ii) the method does not result in a single analytical solution.

The organization of the rest of the paper is as follows. The DC motor model and the uncertain parameters of the DC motor are introduced in Sec. 2. Mapping the robust controller design requirements into the parameter space such as Hurwitz stability, D-stability, phase margin and mixed sensitivity (robust performance) requirements are explained and also design method is applied to DC motor speed control in Sec. 3. The

add-on disturbance observer structure and design methodology are given in Sec. 4. The simulation results are shown in Sec. 5. Experimental set-up is described and experimental results are given in Sec. 6. The paper ends with conclusions in Sec. 7.

2. DC motor modelling and uncertainties

This section describes the DC motor modeling. Fig. 1 shows the DC motor scheme with its electrical and mechanical parts.

Using Kirchhoff's law, the following equation is obtained.

$$V_m = L_m \frac{dI_m}{dt} + R_m I_m + k_i \omega_m \tag{1}$$

where V_m is the voltage from the amplifier which drives the motor, R_m is the motor armature resistance, I_m is the motor armature current, L_m is the motor armature inductance, k_i is the back- EMF constant and ω_m is the motor angular speed.

The dynamics of the motor is given by Newton's second equation with the following equation:

$$J\dot{\omega}_m = k_m I_m + \tau_d \tag{2}$$

where J is the total moment of inertia (motor rotor and the load), τ_d is the disturbance torque and k_m is the motor torque constant. In SI units, the motor torque constant is equal to back-EMF constant, that is $k_i = k_m$. After this, k_m is used for both constants.

Using Eqs. (1) and (2) and assuming $L_m << R_m$ and neglecting the viscous friction in the system, the transfer function $G(s)$ from voltage applied to the motor to motor angular speed can be written as follows:

$$G(s) = \frac{k_m}{R_m\left(Js + \frac{k_m^{\,2}}{R_m}\right)}. \tag{3}$$

The open loop block diagram of the motor with torque disturbance is depicted in Fig. 2.

In the simulations and experiments Quanser DC motor set which includes a Maxon high quality DC motor is used. The nominal parameters of the DC motor used is given at Table 1.

Two parameters k_m and J are taken as uncertain parameters considering ± 20 % uncertainty on nominal values. k_m values are between 0.0402 and 0.0602 Nm/A and J values are between $17.68\text{x}10^{-6}$ and $26.52\text{x}10^{-6}$ kgm^2. An uncertainty box is depicted in Fig. 3 for showing these uncertainties.

3. Design methodology by mapping multi-objective requirements into parameter space

In this section, a robust PI controller design methodology based on parameter space approach is introduced. The mapping of multi-objective design requirements into the parameter space is explained including Hurwitz stability, D-stability, phase margin bounds and frequency domain (mixed sensitivity) bounds mapping. The PI controlled closed loop system can be seen from Fig. 4.

Table 1. The nominal parameters of the DC motor.

Parameter	Value	Unit
k_m	0.0502	Nm/A
J	$22.1\text{x}10^{-6}$	kgm^2
R_m	10.6	Ω

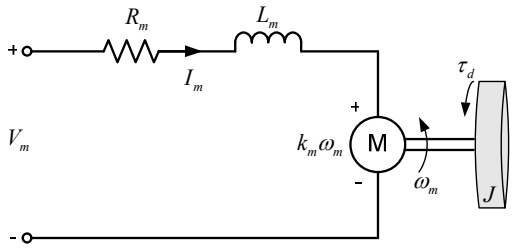

Fig. 1. The DC motor scheme.

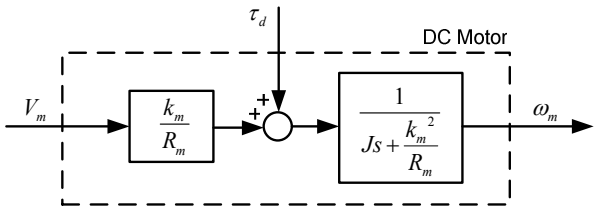

Fig. 2. The open loop block diagram of the dc motor with torque disturbance.

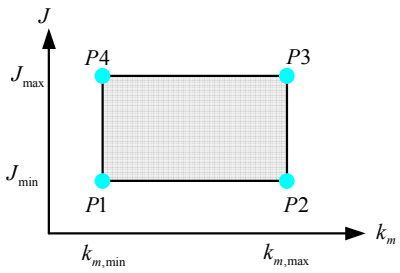

Fig. 3. Uncertainty box for the DC motor parameters.

3.1 Hurwitz stability

Consider the plant is given by

$$G(s) = \frac{N(s)}{D(s)} \tag{4}$$

where N represents the numerator of the plant and D represents the denominator of the plant. The real and imaginer parts of the numerator and denominator can be defined as $N(j\omega) = N_R(j\omega)+N_I(j\omega)$ and $D(j\omega) = D_R(j\omega)+D_I(j\omega)$.

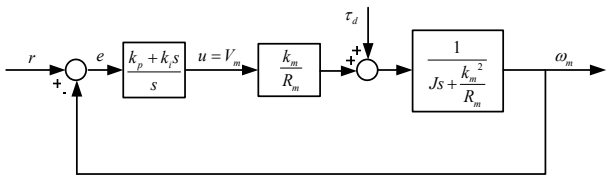

Fig. 4. The PI controlled closed system block diagram.

The PI controlled closed loop system characteristic equation can be written as

$$p_c(s) = sD(s) + (k_p s + k_i)N(s) = a_{n+1}s^{n+1} + a_n s^n + \ldots\ldots + a_1 s + a_0 = 0 \quad (5)$$

where n is the degree of the plant $G(s)$.

The Hurwitz stability boundary crossed by a pair of complex conjugate roots is characterized by the following equations:

$$\mathrm{Re}\left[p_c(j\omega)\right] = 0$$
$$\mathrm{Im}\left[p_c(j\omega)\right] = 0 \text{ for } \forall\omega \in [0, \infty). \quad (6)$$

This is called as Complex root boundary (CRB).

There may be a real root boundary such that a single real root crosses the boundary at frequency $\omega = 0$ is characterized by

$$p_c(0) = 0 \quad \text{or} \quad a_0 = 0. \quad (7)$$

This is called as Real root boundary (RRB).

There may exists an Infinite root boundary (IRB) which is characterized by a degree drop in characteristic polynomial at $\omega = \infty$. This degree drop in characteristic polynomial is characterized as

$$a_{n+1} = 0. \quad (8)$$

CRB, RRB and IRB solutions by parameterizing ω can be plotted into the k_p-k_i parameter plane to show the Hurwitz stability regions of the given closed loop system. The k_p-k_i values which provide Hurwitz stability can be chosen visually from the stable region of the parameter plane.

3.2 D-stability

The aforementioned parameter space computation method to determine Hurwitz stability regions can be extended to specify relative stability regions such as D-stability. A closed loop system is D-stable when the roots of the closed loop characteristic equation lie in the D-stable region in the complex plane as depicted in Fig. 5.

The boundary ∂_1 in Fig. 5 can be mapped into the parameter

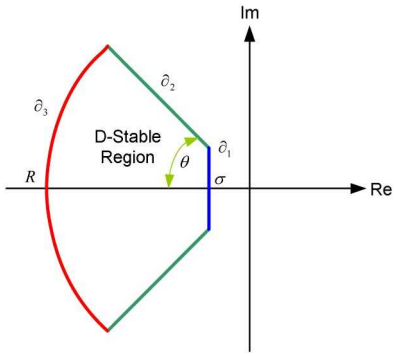

Fig. 5. D-stable region in the complex plane.

space by using $s - \sigma$ instead of s in Eq. (5) in order to shift the stability boundary to ∂_1 in the complex plane. Solving for k_p and k_i in Eq. (6) for CRB and Eq. (7) for RRB, and then plotting results in the k_p-k_i plane will result in the ∂_1 boundary in the parameter space. For ∂_1 boundary, there is no IRB because s is never equal to infinity in the D-shaped region. For mapping ∂_2 boundary, use $re^{j\theta}$ for s in Eq. (5) and parameterize r in Eq. (6) to obtain the CRB of ∂_2. No RRB and IRB solution exists because r is never equal to zero or infinity. Lastly, ∂_3 boundary maps into the parameter space by substituting s with $Re^{j\theta}$ where R is constant and parameterizing over θ in Eq. (5). This results in CRB for changing θ and RRB for $\theta = 0$.

3.3 Phase margin

The constant phase margin can be also plotted in the parameter space. The constant phase margin boundary satisfies the following equation:

$$L(j\omega) = e^{j(m_\phi - \pi)} \quad (9)$$

where L is the loop gain and m_φ is the phase margin bound.

The real and imaginary parts of $L(j\omega)$ can be written as

$$\mathrm{Re}\left[L(j\omega)\right] = \mathrm{Re}\left[C(j\omega)G(j\omega)\right] = \mathrm{Re}\left[\frac{k_p j\omega + k_i}{j\omega}\frac{N_R + jN_I}{D_R + jD_I}\right] = -\cos(m_\phi) \quad (10)$$

and

$$\mathrm{Im}\left[L(j\omega)\right] = \mathrm{Im}\left[C(j\omega)G(j\omega)\right] = \mathrm{Im}\left[\frac{k_p j\omega + k_i}{j\omega}\frac{N_R + jN_I}{D_R + jD_I}\right] = -\sin(m_\phi). \quad (11)$$

From Eqs. (10) and (11), solving for k_p and k_i values result in phase margin bound into the parameter space. Constant gain margin bounds can also be obtained in following similar procedure.

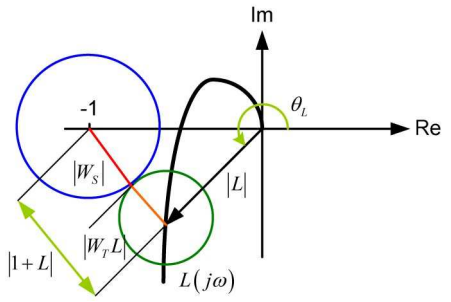

Fig. 6. The point condition for mixed sensitivity.

3.4 Mapping mixed sensitivity (frequency domain) bounds

The aim of this section is to map frequency domain criteria of robust control into the parameter space. Similar to the approach in Refs. [26, 27, 29, 30], a parameter space design based on satisfying the robust performance requirement is used here as follows:

$$\left\| |W_S S| + |W_T T| \right\|_\infty < 1 \text{ or } |W_S S| + |W_T T| < 1, \ \forall \omega \tag{12}$$

where $S = 1/(1+L)$ and $T = L/(1+L)$ are the sensitivity and complementary sensitivity functions and W_S and W_T are corresponding weights.

Mixed sensitivity problem Eq. (12) can also be expressed in the limit as the equality

$$|W_S| + |W_T L| = |1 + L|, \ \forall \omega \tag{13}$$

which is called the point condition at each frequency. The point condition is depicted in Fig. 6.

A circle with origin at -1 and a radius equal to $|W_S(\omega)|$ at a specific frequency ω is drawn first. Loop gain $L(j\omega)$ at the same frequency is shown as vector L with magnitude $|L|$ and angle θ_L in Fig. 6 and is given by

$$L(j\omega) = |L| e^{j\theta_L} . \tag{14}$$

A second circle with origin at $L(j\omega)$ and with a radius equal to $|W_T(\omega)L(\omega)|$ for specific frequency ω is drawn next.

The vector $1+L$ originating at -1 and ending at L in Fig. 6 should be greater than $|W_S|+|W_T L|$ to satisfy the inequality version of the point condition Eq. (13). This point condition needs to be solved at each frequency to find the controller parameter pairs that satisfy it. Solving and graphically intersecting the solution regions for a sufficient large number of frequencies result in the controller parameter space where robust performance is satisfied.

A graphical solution for $|L|$ using the cosine rule for Fig. 6 results in

$$|L| = \frac{-\cos\theta_L + |W_S||W_T| \pm \sqrt{\Delta}}{1 - |W_T|^2} \tag{15}$$

where

$$\Delta = 1 + \cos^2\theta_L - 2|W_S||W_T|\cos\theta_L + |W_S|^2 + |W_T|^2 . \tag{16}$$

The first part of the solution procedure for loop gain L is the formation of a grid of θ_L in [0, 2π] and then solving Eq. (15) for $|L|$ and computing $L = |L| e^{j\theta L}$. Then, L is expressed in terms of a fictitious controller K as follows:

$$L = KG = (K_R + jK_I)G . \tag{17}$$

Solving Eq. (17) for the real and imaginary parts K_R and K_I of the fictitious controller K and then solving

$$K_R + jK_I = \frac{L}{G} = \frac{k_p j\omega + k_i}{j\omega} \tag{18}$$

for PI controller parameters k_p and k_i result in

$$k_p = K_R \tag{19}$$

$$k_i = -K_I \omega \tag{20}$$

which is the final step of the solution.

The aforementioned point condition solution procedure is summarized below.

1. Choose a specific ω value. $|W_S(\omega)|$, $|W_T(\omega)|$ and $G(j\omega)$ at frequency ω are all known at this point.
2. Let $\theta_L \in [0, 2\pi]$. Evaluate Δ using Eq. (16), and select the active range of θ_L, where $\Delta \geq 0$ is satisfied. For all values of θ_L in the active range.
   2.1. Evaluate $|L|$ using Eq. (15). Keep only the positive solutions (since $|L|$ cannot be negative).
   2.2. Evaluate $L = |L| e^{j\theta L}$.
   2.3. Solve for the corresponding fictitious controller real and imaginary parts K_R and K_I in Eq. (17).
   2.4. Substitute for K_R and K_I into the right-hand sides of Eqs. (19) and (20), and solve for k_p and k_i.
3. Plot the closed curve of k_p versus k_i values (for all active θ_L values in 2). Either inside or the outside of this curve is a solution of Eq. (13) at chosen frequency ω. The obtained region is the point condition solution in the chosen controller parameter plane at the frequency chosen in step 1.
4. Go back to step 1, and repeat the procedure at a different frequency.
5. Plot the intersection of all point condition solutions for all frequencies considered. This is the overall solution region for robust performance.

3.5 Application to robust PI DC motor speed control

The aforementioned multi-objective robust controller design methodology was applied to PI DC motor speed control here. D-stability, phase margin and mixed sensitivity boundaries mapping procedure were realized for four operating points (vertices of the uncertainty box) shown in Fig. 3. Then, the common k_p-k_i value that satisfies the design requirements for all points was selected from the k_p-k_i parameter plane.

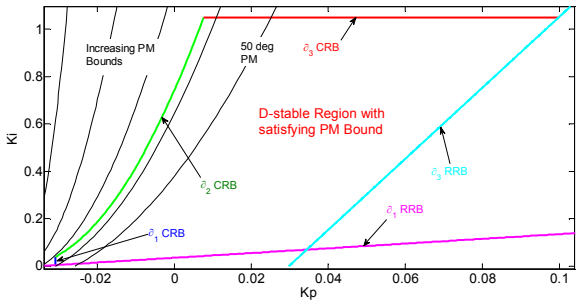

Fig. 7. Detailed view of D-stability and Phase Margin boundaries in parameter space for P1.

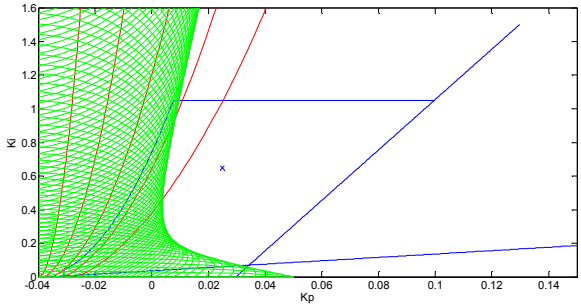

Fig. 8. Solutions for P1 where $k_{m,min}$ = 0.0402, J_{min} = 17.68x10^{-6} (Blue: D-stability boundary, Red: PM Boundary, Green: Mixed Sens. Req. Boundary).

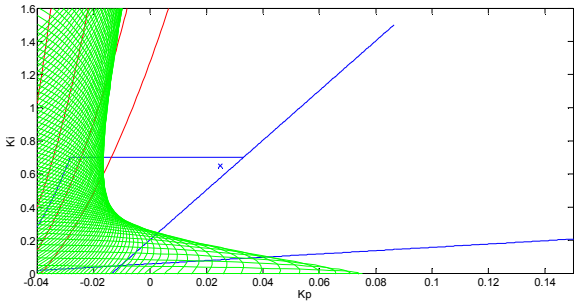

Fig. 9. Solutions for P2 where $k_{m,max}$ = 0.0502, J_{min} = 17.68x10^{-6}.

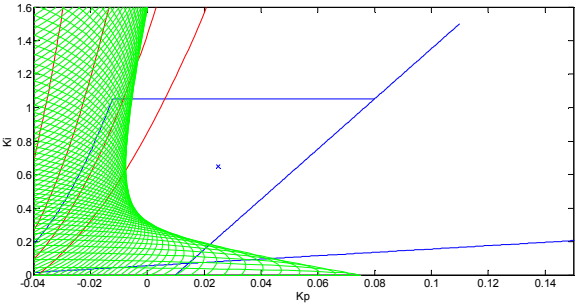

Fig. 10. Solutions for P3 where $k_{m,max}$ = 0.0502, J_{max} = 26.52x10^{-6}.

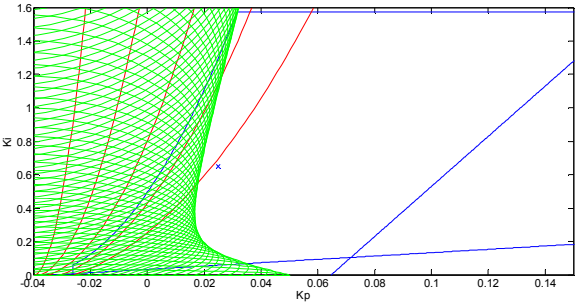

Fig. 11. Solutions for P4 where $k_{m,min}$ = 0.0402, J_{max} = 26.52x10^{-6}.

D-stability requirements were determined as follows: No roots can be closer than -1 to the Im axis (σ = 1) and no roots can be further than -15 (R = 15), a maximum damping can be 70 degree (θ = 70^{o}) which corresponding to a damping ratio of 0.342.

Phase margin can be at least 50 degree (PM ≥ 50 deg).

Fig. 7 shows the solution regions for D-stability and phase margin requirements in parameter space. ∂_1 CRB and RRB, ∂_2 CRB and ∂_3 CRB of D-stability and the increasing phase margin bounds depicted. The intersection of bounds determined the D-stable region with satisfying required PM bound.

In order to map robust performance criteria into the parameter space, firstly the sensitivity and the complementary sensitivity weights were determined. The inverse of the sensitivity function weight is selected as

$$W_S^{-1} = h_s \frac{s + \omega_s l_s}{s + \omega_s h_s}. \quad (21)$$

With l_s = 0.5 (i.e., less than 50 % steady state error) being the low frequency bound, h_s = 4 being the high frequency bound, and ω_s = 4 rad/sec being the approximate bandwidth.

The complementary sensitivity function weight is chosen as

$$W_T = h_T \frac{s + \omega_T l_T}{s + \omega_T h_T} \quad (22)$$

where the low frequency gain is l_T = 0.2, the high frequency gain is h_T = 1.8 (corresponds to uncertainty of up to 180 % at high frequencies), and the frequency of transition to significant model uncertainty is ω_T = 4 rad/sec.

The mixed sensitivity requirement for the selected weights was mapped into the parameter space. The results with including D-stability and phase margin boundaries can be seen from Figs. 8-11 for the points P1, P2, P3 and P4 shown in Fig. 3. Blue lines restricted the parameter space for D-stability, red lines restricted for PM bounds and green lines restricted the parameter space for mixed sensitivity requirements.

The common k_p and k_i were selected as (0.025, 0.65), these points satisfies all design requirements for all operating points. These controller parameters were used in all of the simulation.

Table 2 shows the closed loop pole locations and phase margin values for four operating points. The closed loop poles are in the D-stable region (shown in Fig. 12) and the phase margin requirement is satisfied, all phase margins is larger than 50 degree.

Fig. 13 shows the $|W_S S|+|W_T T|$ frequency-domain plots for all four points as a function of frequency. It is clear from this

Table 2. Closed loop pole locations and phase margin values for four vertices of the uncertainty box.

Points	Closed loop pole locations	Phase margin [deg]
1	-6.9929 + 9.5146i -6.9929 – 9.5146i	61.1032
2	-13.6842 + 4.6411i -13.6842 – 4.6411i	83.5883
3	-9.1228 + 7.4815i -9.1228 – 7.4815i	73.8756
4	-4.6619 + 8.4391i -4.6619 – 8.4391i	51.5451

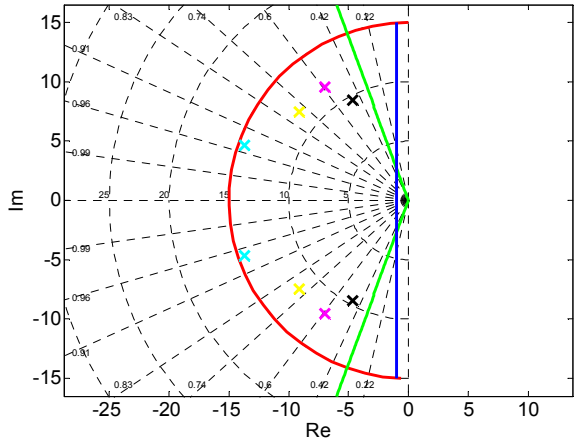

Fig. 12. Closed loop poled locations and D-stability region.

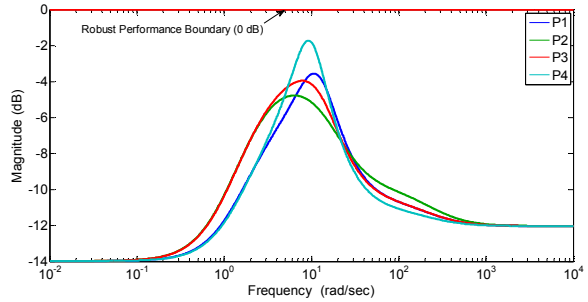

Fig. 13. Robust performance plots $|W_S S|+|W_T T|$.

figure that constraint Eq. (12) is satisfied at each of the different operating points in Fig. 3 and for the chosen controller parameters, as none of the plots touch the 0-dB ($|W_S S|+|W_T T| = 1$) line.

4. Improvement on system response using disturbance observer

4.1 Add-on disturbance observer structure

The disturbance observer is a well-known approach in the mechatronic systems control area that is used to achieve insensitivity to modeling error and disturbance rejection. It was introduced by Ref. [32] and further refined by Ref. [33]. It has been used successfully in a variety of mechatronics applications. For instance, friction compensation in Ref. [34], road vehicle yaw stability control in Refs. [27-30], robust atomic force microscope control in Ref. [35], power assisted electric bicycle control in Ref. [36], table drive system in Ref. [20], hard-disc-drive servo system in Ref. [37] and heavy vehicle rollover prevention [38]. In the disturbance observer approach, the inverse of the desired or nominal plant model is used to observe the disturbances and to cancel the effect of disturbances in the control signal. As a result, the closed system is forced to act like its nominal or desired model. The system structure with add-on disturbance observer is depicted in Fig. 14.

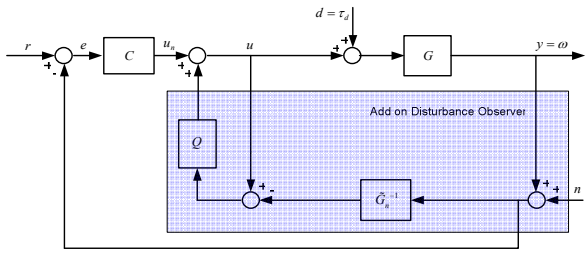

Fig. 14. The system structure with add-on disturbance observer.

Consider plant G with multiplicative uncertainty Δ_m and input disturbance d:

$$y = G(u + d) \tag{23}$$

where $G = G_n(1+\Delta_m)$ and G_n is the nominal model of the plant.

The aim in the disturbance observer usage is to obtain

$$y = G_n u_n \tag{24}$$

where u_n is the new control input.

This aim can be achieved in disturbance observer design by treating the external disturbance and model uncertainty as an extended disturbance e and solving for it as

$$y = G_n u + \underbrace{G_n d + G_n u\Delta_m + G_n d\Delta_m}_{e} \tag{25}$$

$$e = y - G_n u \tag{26}$$

and using the new control signal u_n given by

$$u = u_n - \frac{1}{G_n} e = u_n - \frac{1}{G_n} y + u \tag{27}$$

to approximately cancel its effect when substituted in Eq. (25). With the aim of not to overcompensate at high frequencies and to avoid stability robustness problems, the feedback signals in Eq. (27) are multiplied by the low pass filter Q. In this case, the final equation becomes

$$u = u_n - Q\left(\frac{1}{G_n}(y+n)+u\right) \tag{28}$$

where n represents the sensor noise and, it is available for the case of real implementation.

The disturbance observer can be designed both in continuous time and discrete time. For discrete time design, please refer to Ref. [39]. In discrete time implementation, if $G_n(z)$ is a minimum phase system, its inverse can directly be assigned, if not, stable version of $\tilde{G}_n^{-1}(z)$ can be obtained using Input shaping filter (ISF) designing techniques such as Zero phase error tracking control (ZPETC), Precision tracking control (PTC), Optimal precision tracking control (OPTC).

The loop gain of the disturbance observer compensated plant is

$$L = \frac{GQ}{G_n(1-Q)} \tag{29}$$

with the model regulation, disturbance rejection and sensor noise rejection transfer functions given by

$$\frac{y}{u_n} = \frac{G_n G}{G_n(1-Q)+GQ} \tag{30}$$

$$\frac{y}{d} = \frac{1}{1+L} = \frac{G_n(1-Q)}{G_n(1-Q)+GQ} \tag{31}$$

$$\frac{y}{n} = \frac{-L}{1+L} = \frac{-GQ}{G_n(1-Q)+GQ}. \tag{32}$$

It is seen that Q must be a unity gain low pass filter. This choice will result in $y/u_n \to G_n$, $y/d \to 0$ at low frequencies where $Q \to 1$ and $y/n \to 0$ at high frequencies where $Q \to 0$.

There are limitations in the selection of the bandwidth of the Q filter. First of all, the bandwidth of the Q filter cannot exceed the bandwidth of the actuator used. Another limitation for the Q filter arises from the robust stability requirement.

The characteristic equation of the disturbance observer compensated system can be written

$$G_n(1-Q)+G_n(1+\Delta_m)Q = 0 \tag{33}$$

as

$$G_n(1+\Delta_m)Q = 0 \;\rightarrow\; Q = -\frac{1}{\Delta_m} \tag{34}$$

and note that when the presence of Δ_m does not change the number of unstable poles and zeros of G in comparison to those of G_n, the application of the Nyquist stability criterion results in

$$|Q| < \left|\frac{1}{\Delta_m}\right|, \ \forall\omega \tag{35}$$

as the necessary and the sufficient condition for robust stability.

The feedback controller C also affects the robust stability of the overall system. In the presence of the feedback control as shown in Fig. 14, the closed loop system, disturbance rejection and sensor noise rejection transfer functions can be written as

$$\frac{y}{r} = \frac{CG_nG}{G_n(1-Q)+G(CG_n+Q)} \tag{36}$$

$$\frac{y}{d} = \frac{G_n(1-Q)}{G_n(1-Q)+G(CG_n+Q)} \tag{37}$$

$$\frac{y}{n} = \frac{-G(CG_n+Q)}{G_n(1-Q)+G(CG_n+Q)}. \tag{38}$$

In the case of feedback control, the characteristic equation of the closed loop system can be written by

$$G_n(1-Q)+G_n(1+\Delta_m)(CG_n+Q) = 0 \tag{39}$$

as

$$\frac{Q+CG_n}{1+CG_n} = -\frac{1}{\Delta_m} \tag{40}$$

and using the Nyquist stability criterion results in

$$\left|\frac{Q+CG_n}{1+CG_n}\right| < \left|\frac{1}{\Delta_m}\right|, \ \forall\omega \tag{41}$$

as the necessary and the sufficient condition for robust stability including feedback control shown in Fig. 14. Thus, robust stability condition of the system can be investigated in the absence and presence of the feedback control using Eqs. (35) and (41), respectively.

4.2 Disturbance observer design

Using the stability robustness conditions given in Eqs. (35) and (41), the cut-off frequency of the low pass Q filter is determined. The multiplicative uncertainty Δ_m is calculated using $\Delta_m = (G_p - G_n)/G_n$. Here the plant G_p is taken different as Eq. (3) in order to add the effect of the unmodelled dynamics by considering L_m the motor armature inductance in the investigation of stability robustness. Therefore, the plant model G_p is taken as follows:

$$G_p(s) = \frac{k_m}{\left(Js+\frac{k_m^2}{R_m}\right)(L_m s+R_m)} e^{-sh}. \tag{42}$$

Also, time delay h is considered to reflect the other unmod-

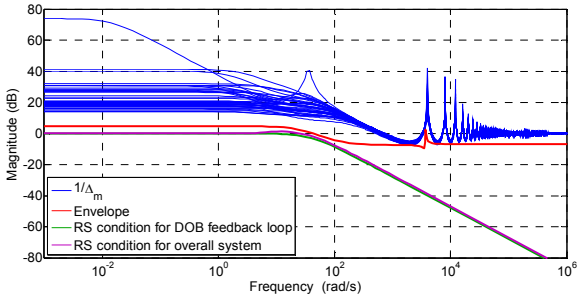

Fig. 15. Stability robustness plot.

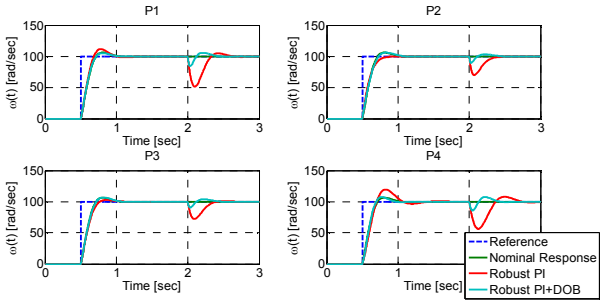

Fig. 16. Step response and step disturbance rejection simulation results.

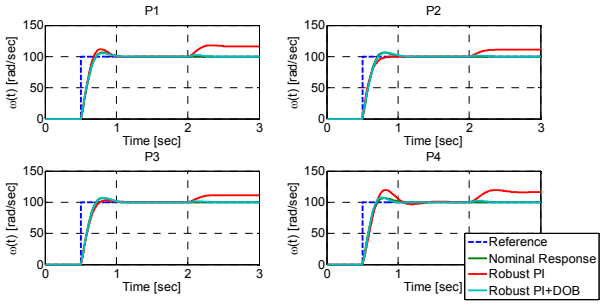

Fig. 17. Step response and ramp disturbance rejection simulation results.

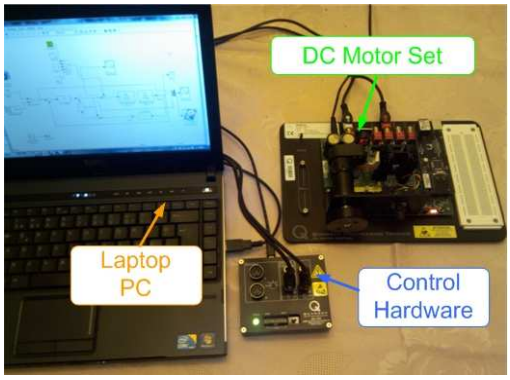

Fig. 18. Experimental setup.

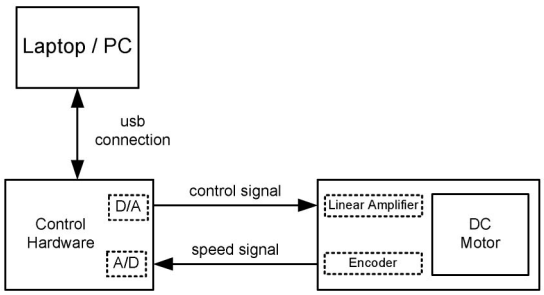

Fig. 19. Schematic diagram of the experimental setup.

elled dynamics. Time delay h is selected as 1.5 times of sampling time. The feedback motor angular speed is calculated based on encoder measurements. Since the angular speed is determined by taking differences of the angles between two sampling intervals, there is a delay of a one sampling time. Also, there is an effect of controller hardware dynamics, it is approximated as an extra delay corresponding to half a sampling time [40].

The uncertainty for k_m and J shown in Fig. 3 is divided into an equally spaced grid of values in both axis directions and the $1/\Delta_m$ plot shown in Fig. 15 is obtained. An envelope is drawn to determine the upper bound of the multiplicative uncertainty. Using these plots and considering stability robustness conditions Eqs. (35) and (41), Q is selected as a first order low pass filter of $1/(T_q s+1)$ with the cut-off frequency of 40 rad/sec.

5. Simulation results

Simulations were performed to show the effectiveness of the parameter space based fixed robust PI speed controller and the designed add-on disturbance observer. Figs. 16 and 17 show the step input response of desired angular velocity of 100 rad/sec for four operating points shown in Fig. 3. A step disturbance was applied to the system at time = 2 sec for simulation shown in Fig. 16 and, a ramp disturbance was applied to the system at time = 2 sec for simulation shown in Fig. 17. Results show that robust PI plus disturbance observer system rejects step and ramp disturbance successfully and forces the uncertain system to act as nominal plant while satisfying multi-objective design requirements.

6. Experiments

6.1 Experimental set-up

Fig. 18 shows the experimental setup. Also, schematic diagram of the experimental setup is depicted in Fig. 19. The main part of the experimental setup is a 15 Watt motor of Maxon brand equipped with a quadrature encoder with the resolution of 4096 pulses per revolution. The encoder pulses are received by a 24-bit encoder counter integrated circuit. The angular speed of the motor for feedback is derived from encoder signal. A linear 15 V, 1.5 A power amplifier is used to drive the motor. Quanser Q2-usb board is used as control hardware. The control signal to the DC motor linear amplifier is sent from a 12 bit D/A convertor on Q2-usb board and the angular speed signal is received by a 12 bit A/D convertor on Q2-usb board. The control algorithms is prepared on Mat-

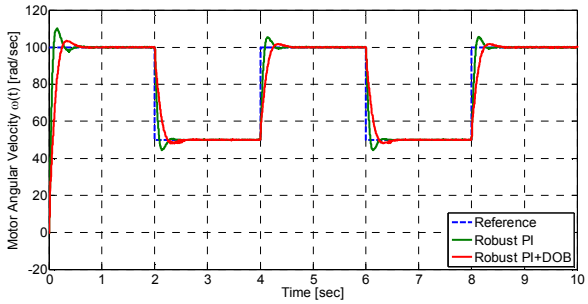

Fig. 20. Trajectory tracking experiment result.

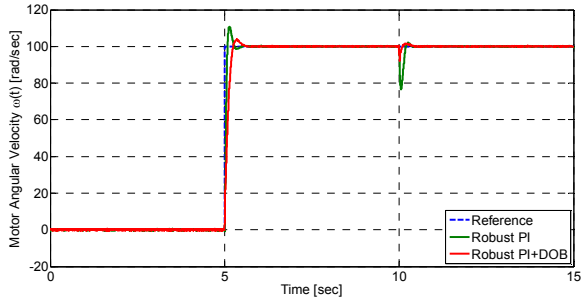

Fig. 21. Step disturbance rejection experiment result.

lab/Simulink environment and realized with a 2.27 GHz Intel Core i5 processor Laptop PC. The control algorithms are embedded to Q2-usb board using Matlab real time windows target and Quanser QUARC software. The DC motor is controlled at the sample rate of 1 kHz.

6.2 Experimental results

Three different experiments were conducted in order to test the proposed control scheme. Fig. 20 shows the trajectory tracking experiment results. The reference motor angular velocity was changing from 100 rad/sec to 50 rad/sec in 2 secs with initial velocity of 100 rad/sec. The robust PI plus disturbance observer control system tracks the reference signal with less overshoot with respect to only robust PI control system. However, rise time of the robust PI plus DOB system is longer. When the disturbance observer added to the system, also an extra dynamics inserted to the system, this situation was arisen from this fact. Fig. 21 shows the step disturbance rejection test result. At time = 10 sec, the step disturbance was applied to the system. It can be seen that the robust PI plus DOB system attenuated the step disturbance better than only robust PI control system. Fig. 22 shows the ramp disturbance rejection test result. The ramp disturbance was injected to the system at time = 10 sec. The only robust PI control system could not attenuate the ramp disturbance but the robust PI plus DOB system dealt with the ramp disturbance successfully.

7. Conclusions

The parameter space approach based robust PI controller

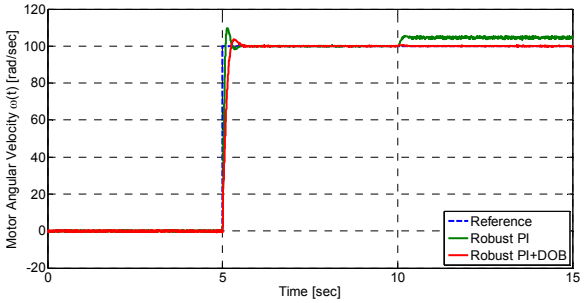

Fig. 22. Ramp disturbance rejection experiment result.

and add on disturbance observer design for the DC motor speed control has been presented here. The motor torque constant and total moment of inertia of DC motor has been taken as uncertain parameters. Multi-objective design requirements such as D-stability, phase margin and mixed sensitivity (frequency domain) bounds have been mapped into the controller parameter space to find the robust PI controller coefficients. In order to improve the tracking performance and disturbance rejection properties of the proposed control system, add on disturbance observer has been employed. The disturbance observer design procedure considering stability robustness of the overall system has been given in details. The proposed control system has been tested through simulations and experiments successfully.

References

[1] L. Zollo, S. Roccella, E. Guglielmelli, M. C. Carrozza and P. Dario, Biomechatronic design and control of an anthropomorphic artificial hand for prosthetic and robotic applications, *IEEE/ASME Transactions on Mechatronics,* 12 (4) (2007) 418-429.

[2] S.-F. Yang and J.-H. Chou, A mechatronic positioning system actuated using a micro DC-motor-driven propeller-thruster, *Mechatronics,* 19 (2009) 912-926.

[3] Q. Huang, Z. Huang and H. Zhou, Nonlinear optimal and robust speed control for a light-weighted all-electric vehicle, *IET Control Theory and Applications,* 3 (4) (2009) 437-444.

[4] S. Kim, J. Kim, G. Sung and J. Lee, Evaluation and development of improved braking model for a motor-assisted vehicle using Matlab/Simulink, *Journal of Mechanical Science and Technology*, 29 (7) (2015) 2747-2754.

[5] W. Wu, DC motor drive speed regulation: using a repetitive control application in a flatbed scanner, *IEEE Industry Applications Magazine,* 18 (2) (2012) 38-46.

[6] S. V. Ambesange, S. Y. Kamble and D. S. More, Application of sliding mode control for the speed control of DC motor drives, *Proc. of IEEE International Conference on Control Applications (CCA),* Hyderabad, India (2013) 832-836.

[7] M. Yasoobi, A. Khosravi and A. Lari, Mixed H_2/H_∞ fixed structure speed control of DC motor using IPSO algorithm, *Proc. of the 2nd International Conference on Control, Instrumentation and Automation (ICCIA),* Shiraz, Iran (2011)

451-456.

[8] G. Murtaza and A. I. Bhatti, Control of DC motors using sliding mode, *Proc. of 9th International Bhurban Conference on Applied Sciences and Technology (IBCAST)*, Islamabad, Pakistan (2012) 37-42.

[9] J. Y. Hung, R. M. Nelms and P. B. Stevenson, An output feedback sliding mode speed regulator for DC drives, *IEEE Transactions on Industry Applications,* 30 (3) (1994) 691-698.

[10] S.-Y. Chang, P.-H. Yu and W.-C. Su, Pre- and post-filtering approach to sensorless VSS speed control of a permanent magnet DC motor subject to Hammerstein and Wiener nonlinearities, *Control Engineering Practice,* 21 (2013) 1577-1583.

[11] P. Cepeda, P. Ponce and A. Molina, A novel speed control for DC motors: Sliding mode control, fuzzy inference system, neural networks and genetic algorithms, *Proc. of the 11th Mexican International Conference on Artificial Intelligence (MICAI),* San Luis Potosi, Mexico (2012) 116-121.

[12] R. Lu, S. Li and L. Xue, Robust H-inf optimal speed control of DC motor using LMI approach, *Proc. of the 20th Chinese Control and Decision Conference (CCDC),* Yantai, Shandong (2008) 4350-4354.

[13] A. A. El-Samahy, Speed control of DC motor using adaptive variable structure control, *Proc. of IEEE 31th Annual Power Electronics Specialists Conference (PESC),* Galway, Ireland (2000) 1118-1123.

[14] M. A. El-Sharkawi and S. Weerasooriya, Development and implementation of self-tuning tracking controller for DC motors, *IEEE Transactions on Energy Conversion,* 5 (1) (1990) 122-128.

[15] M. A. Rahman and M. A. Hoque, On-line self-tuning ANN-based speed control of a PM DC motor, *IEEE/ASME Transactions on Mechatronics,* 2 (3) (1997) 169-178.

[16] B. Bhushan and M. Singh, Adaptive control of DC motor using bacterial foraging algorithm, *Applied Soft Computing,* 11 (2011) 4913-4920.

[17] J. Peng and J. R. Dubay, Identification and adaptive neural network control of a DC motor system with dead-zone characteristics, *ISA Transactions,* 50 (2011) 588-598.

[18] C. I. Muresan, S. Folea, G. Mois and E. H. Dulf, Development and implementation of a FPGA based fractional order controller for a DC motor, *Mechatronics,* 23 (2013) 798-804.

[19] C. J. Kempf and S. Kobayashi, Disturbance observer and feedforward design for a high-speed direct-drive positioning table, *IEEE Transactions on Control Systems Technology,* 7 (5) (1999) 513-526.

[20] T. Satoh, K. Kaneko and N. Saito, Improving tracking performance of predictive functional control using disturbance observer and its application to table drive systems, *International Journal of Computers, Communications and Control,* 7 (3) (2012) 550-564.

[21] B. Rashidi, M. Esmaeilpour and M. R. Homaeinezhad, Precise angular speed control of permanent magnet DC motors in presence of high modeling uncertainties via sliding mode observer-based model reference adaptive algorithm, *Mechatronics,* 28 (2015) 79-95.

[22] N. Matiyali and R. Potluri, Disturbance observer for multivariable speed-dependent disturbance in DC motors, *Proc. of IEEE Indian Control Conference,* Hyderabad, India (2016) 105-110.

[23] G. Shahgholian, M. Maghsoodi, M. Mahdavian, M. Janghorbani, M. Azadeh and S. Farazpey, Analysis of speed control in DC motor drive by using fuzzy control based on model reference adaptive control, *Proc. of the 13th International Conference on Electrical Engineering/Electronics, Computer, Telecommunications and Information Technology (ECTI-CON),* Chiang Mai, Thailand (2016).

[24] C. Hongqing, T. Weinan, G. Binzhao, L. Qifang and C. Hong, Speed control of the permanent-magnet DC motor subjected to uncertainty and disturbance, *Proc. of the 35th Chinese Control Conference*, Chengdu, China (2016) 4664-4669.

[25] J. Ackermann, P. Blue, T. Bunte, L. Güvenç, D. Kaesbauer, M. Kordt, M. Mühler and D. Odental, *Robust control: The parameter space approach,* Springer-Verlag, London, UK (2002).

[26] L. Güvenç and J. Ackermann, Links between the parameter space and frequency domain methods of robust control, *International Journal of Robust and Nonlinear Control,* 11 (15) (2001) 1435-1453.

[27] B. Aksun-Güvenç, T. Bünte, B. Odenthal and L. Güvenç, Robust two degree-of-freedom vehicle steering controller design, *IEEE Transactions on Control Systems Technology,* 12 (4) (2004) 627-636.

[28] S. Öncü, S. Karaman, L. Güvenç, S. S. Ersolmaz, E. S. Öztürk, E. Çetin and M. Sinal, Robust yaw stability controller design for a light commercial vehicle using a hardware in the loop steering test rig, *Proc. of IEEE Intelligent Vehicle Symposium,* İstanbul, Turkey (2007) 852-859.

[29] B. Aksun-Güvenç, L. Güvenç and S. Karaman, Robust yaw stability controller design and hardware-in-the-loop testing for a road vehicle, *IEEE Transactions on Vehicular Technology*, 58 (2) (2009) 555-571.

[30] B. Aksun-Güvenç, L. Güvenç and S. Karaman, Robust MIMO disturbance observer analysis and design with application to active car steering, *International Journal Robust and Nonlinear Control,* 20 (2010) 873-891.

[31] B. Demirel and L. Güvenç, Parameter space design of repetitive controllers for satisfying a robust performance requirement, *IEEE Transactions on Automatic Control,* 55 (8) (2010) 1893-1899.

[32] K. Ohnishi, A new servo method in mechatronics, *Transactions of Japanese Society of Electrical Engineering,* 107-D (1987) 83-86.

[33] T. Umeno and Y. Hori, Robust speed control of dc servomotors using two degrees-of-freedom controller design, *IEEE Transactions on Industrial Electronics,* 38 (5) (1991) 363-368.

[34] L. Güvenç and K. Srinivasan, Friction compensation and

evaluation for a force control application, *Journal of Mechanical Systems and Signal Processing,* 8 (6) (1994) 623-638.

[35] B. Aksun-Güvenç, S. Necipoğlu, B. Demirel and L. Güvenç, Mechatronics, J. Paulo Davim (Ed.), *Robust Control of Atomic Force Microscopy,* Wiley-ISTE (2013) 103-132.

[36] X. Fan and M. Tomizuka, Robust disturbance observer design for a power-assist electric bicycle, *Proc.of IEEE American Control Conference,* Baltimore, MD, USA (2010) 1166-1171.

[37] Y. Luo, T. Zhang, B. J. Lee, C. Kang and Y. Q. Chen, Disturbance observer design with Bode's ideal cut-off filter in hard-disc-drive servo system, *Mechatronics,* 23 (7) (2013) 856-862.

[38] F. Yakub, S. Lee and Y. Mori, Comparative study of MPC and LQC with disturbance rejection control for heavy vehicle rollover prevention in an inclement environment, *Journal of Mechanical Science and Technology*, 30 (8) (2016) 3835-3845.

[39] B. Aksun-Güvenç and L. Güvenç, Robust two degree-of-freedom add-on controller design for automatic steering, *IEEE Transactions on Control Systems Technology,* 10 (1) (2002) 137-148.

[40] K. Aström, J. Apkarian and H. Lacheray, *Quanser Engineering Trainer (QET) Series: DC Motor Control Trainer (DCMCT) manual* (2006).

Mümin Tolga Emirler received the Ph.D. degree in mechanical engineering from İstanbul Technical University, İstanbul, Turkey in 2015. He worked previously in the Ohio State University as a postdoctoral researcher. He joined Okan University in February 2016 as an Assistant Professor in the Department of Mechanical Engineering. His current research interests include applied robust control, vehicle dynamics control, control problems in automated / connected vehicles and mechatronic systems.

Bilin Aksun Güvenç received the Ph.D. degree in mechanical engineering from İstanbul Technical University, İstanbul, Turkey in 2001. She worked previously in İstanbul Technical University and Okan University where she was a Professor. She joined the Ohio State University in September 2014 as a Visiting Professor in the Department of Mechanical and Aerospace Engineering and the Center for Automotive Research. Her expertise is in automotive control systems such as yaw stability control, cooperative adaptive cruise control, collision avoidance systems, autonomous vehicles, and smart cities. She is the author of one book, two book chapters and ninety publications in journals and conferences.